J. Fluid Mech. (2008), *vol.* 595, *pp.* 491–507.
doi:10.1017/S0022112007009433 Printed in the United Kingdom

Stability of flows past a pair of circular cylinders in a side-by-side arrangement

J. MIZUSHIMA AND Y. INO

Department of Mechanical Engineering, Doshisha University, Kyotanabe, Kyoto 610-0321, Japan

(Received 17 March 2007 and in revised form 3 October 2007)

The stability and transition of flow past a pair of circular cylinders in a side-by-side arrangement are investigated by numerical simulations and linear stability analyses. Various flow patterns around the cylinders have been reported to appear due to an instability of the steady symmetric flow that is realized at small Reynolds numbers, among which deflected oscillatory flow is particularly noticeable. The physical origin of the flow is explored by bifurcation analyses of the numerical data. We found that the deflected oscillatory flow arises from the steady symmetric flow through sequential instabilities due to stationary and oscillatory unstable modes. Steady asymmetric flow with respect to the streamwise centreline between the two cylinders was also found to be induced by the instability due to a stationary mode in a very narrow range of the gap width between the two cylinders. We classify the instability modes of the steady symmetric flow into four groups in the parameter space of the gap width, and evaluate the critical Reynolds number for each mode of instability.

1. Introduction

Flow past two circular cylinders has been found to exhibit various flow patterns in spite of its simple configuration and to have complex characteristics depending on the arrangement of the cylinders and the Reynolds number (Zdravkovich 1977; Zdravkovich & Pridden 1977; Ohya, Okajima & Hayashi 1988). Among various arrangements, two typical configurations, i.e. tandem and side-by-side, have been investigated extensively. It is known that the drag and lift coefficients on the cylinders exhibit a discontinuous jump at some critical spacing between the two cylinders in a tandem arrangement; the downstream cylinder experiences a complex force from the wake of the upstream cylinder (Ishigai, Nishikawa & Cho 1972; Mizushima & Suehiro 2005). The patterns and oscillation frequencies in the flow past two cylinders in a side-by-side arrangement have been studied, and various flow patterns have been reported depending on the gap width between the cylinders and the Reynolds number; the asymmetric flow past two symmetrically arranged cylinders has received the attention of researchers.

Early research on flow past two cylinders in a side-by-side arrangement has been mostly at large Reynolds numbers ($Re = 10^3 \sim 10^5$) in experiments (Spivack 1946; Ishigai *et al.* 1972; Bearman & Wadcock 1973). Though some scatter is seen in these experimental results, it was found that there exist three distinct regimes of flow depending on the gap between the cylinders. For gaps larger than one diameter, the vortex shedding frequency is the same as that for a single cylinder though synchronization was observed in shedding of vortices from the two cylinders, whereas for gaps less than 0.5 diameter the flow is similar to that past a single bluff body

having the equivalent length scale of the sum of twice the diameter and the gap width. For intermediate gap width between 0.5 and 1.0 diameter, the flow is deflected towards one cylinder and becomes asymmetric, having narrow and wide wakes, and two distinct predominant frequencies are detected in the flow. The higher frequency is observed in the narrow wake and the lower in the wide wake. The deflected flow is unsteady and switches randomly between two asymmetric states. This deflected flow and the two different frequencies have been confirmed in many other papers (Kim & Durbin 1988; Sumner *et al.* 1999; Zhou *et al.* 2001; Zhou, Zhang & Yiu 2002) and it is believed that the higher shedding frequency is a multiple (twice or triple) of the lower frequency for large Reynolds number flows, though the ratio is dependent on the Reynolds number.

The mechanism and behaviour of the flip-flopping of the deflected flow were investigated by Kim & Durbin (1988). They confirmed that transitions between the two asymmetric states can be described as a Poisson stochastic process, and concluded that the flip-flopping may be interpreted as the behaviour of a simple dynamical system with two quasi-stable states although the detailed mechanism that is responsible for the asymmetry and flip-flopping cannot be surmized. The origins of the flip-flopping and the deflection of the flow were sought in analogy with coupled oscillators by Le Gal *et al.* (1990), and later a model of coupled Landau equations was proposed to describe the oscillation in the two wakes by Peschard & Le Gal (1996) which reproduced most of the experimental features such as in-phase and antiphase oscillatory states and an asymmetric bistable locked state. In spite of many attempts to clarify the origin of the deflection of the flow, no clear explanation has been given, except a conjecture by Ishigai, Nishikawa & Cho (1972) that the deflection is induced by a Coanda effect. However, the conjecture was disproved by Williamson (1985), who confirmed the deflection of the flow experimentally by using flat plates in place of two circular cylinders.

The Coanda effect expresses the tendency of a stream to stay attached to a convex surface and does not explain deflection of flow through a gap between two circular cylinders, but predicts a straight stream broadening in accordance with the expansion of the path between the cylinders. A similar flow deflection was also observed in the flow past an array of square cylinders (Le Gal *et al.* 1996), for which the mechanism of the deflection was clarified as the instability of symmetric flow, and the transition from symmetric to confluent flow with stream deflections was explained by a pitchfork bifucation by Mizushima & Takemoto (1996) and Mizushima & Kawaguchi (2000). Although an array of square or circular cylinders may be thought to be similar to two side-by-side cylinders if only one pair in the array of cylinders is focused, the flow past two side-by-side cylinders is not expected to have a pitchfork bifurcation because flow past isolated obstacles such as the pair is expected to become oscillatory due to instability.

The flow characteristics depend on the gap width between the two cylinders. Research has been directed mostly to the gap-width dependence of the flow pattern and the physical characteristics of the flow, and the effect of the Reynolds number on the flow patterns and measured physical quantities have not been considered in detail. Therefore, no definite conditions for the occurrence of synchronized vortex shedding in phase or in antiphase has been obtained from experiments at large Reynolds numbers. Williamson confirmed in his experiment at relatively small Reynolds numbers, ranging from 40 to 160, that vortex shedding from a pair of cylinders is synchronized in phase or in antiphase to form different vortex streets. It was shown that two antiphase vortex streets were formed as the result of antiphase vortex shedding, although in-phase vortex shedding did not yield two stable in-phase vortex streets but led to the

development of a single large-scale wake. Akinaga & Mizushima (2005) applied the linear stability theory to evaluate the critical Reynolds numbers for both the modes of instability, and determined the critical gap width as 2.34 times the diameter of the cylinders. For larger gap width than this critical value, the flow exhibits antiphase oscillation, and in-phase oscillation is observed for smaller gap width although the origin of the deflected oscillatory flow was not addressed in their paper.

Xu, Zhou & So (2003) investigated the influence of the Reynolds number as well as the gap width on the flow structure in detail for the wide range of Reynolds number of 150–14300, using laser-induced fluorescence flow visualization, PIV (particle image velocimetry) method and hot-wire velocimetry. They found that, as the Reynolds number increases, the flow structure in the wake behind the cylinders changes from one vortex street to two streets, one narrow and the other wide, having different oscillation frequencies for gap distances larger than a certain value about 0.25 times the diameter. Only one vortex street like von Kármán's vortex street is realized for distances smaller than the critical value. The one-street flow structure is dominated by one non-dimensional frequency (Strouhal number) $f_0 \sim 0.09$, whereas two frequencies, $f_0 \sim 0.3$ and 0.09, characterize the two-vortex flow structure. Thus it has been shown that the flow structure is dependent on the Reynolds number. Ravoux, Nadim & Haj-Hariri (2003) found various vortex shedding patterns including quasi-periodic, asymmetric and chaotic regimes in their numerical results and classified the patterns in a parameter space consisting of the gap width and the Reynolds number by depicting phase portraits of the cylinder lift and drag coefficients, together with a spectral analysis of the data.

Similar flip-flopping flows as well as in-phase and antiphase synchronized vortex shedding were also observed in flow around two square cylinders placed side-by-side in a numerical simulation using the lattice-Boltzmann method by Agrawal, Djenidi & Antonia (2006), though the critical gap width for the transition from synchrozied flow to flip-flopping flow is much larger than the case of two circular cylinders. They applied a numerical technique called linear stochastic estimate (LSE) to educe the underlying modes in flip-flopping flow and found evidence for both in-phase and antiphase locked vortices, from which they concluded that the flip-flopping regime is in a quasi-stable state between these two modes.

Kang (2003) numerically simulated the flow at small Reynolds numbers, $Re = 40 \sim 160$, and found that the flow characteristics significantly depend on the Reynolds number as well as the gap width. He classified the flow into six flow patterns depending on the Reynolds number and the spacing between the two cylinders, in which deflected oscillatory flow is included.

In spite of many results on the flow past two cylinders in a side-by-side arrangement, the origin of the deflected flow has not been fully examined in detail. We investigate the stability and transition of the flow by numerical simulations and stability analyses in the present paper. Our major objective is to explore the origin of various flow patterns, specifically of the deflected oscillatory flow.

2. Mathematical formulation and boundary conditions

Consider the flow past two circular cylinders placed side by side in a uniform flow with velocity U as illustrated in figure 1. The two circular cylinders have the same diameter d, and the gap width between them is ℓ. We take the x-axis in the direction of the uniform upstream flow and the y-axis perpendicularly to it. Taking d and U as the representative length and velocity scales, we define the gap ratio Γ and

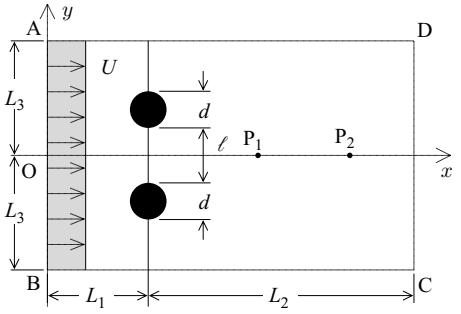

FIGURE 1. Configuration and coordinates.

the Reynolds number Re as $\Gamma \equiv \ell/d$ and $Re \equiv Ud/\nu$, respectively. Here, ν is the kinematic viscosity.

Assuming an incompressible two-dimensional flow field and employing the stream function $\psi(x, y, t)$ and the vorticity $\omega(x, y, t)$ formulation, we write the governing equations of the flow, i.e. the vorticity transport and Poisson equations, in non-dimensional form as

$$\frac{\partial \omega}{\partial t} = \mathcal{N}(\psi, \omega) + \frac{1}{Re}\mathcal{M}\omega, \tag{2.1}$$

$$\omega = -\mathcal{M}\psi, \tag{2.2}$$

$$\mathcal{N}(\psi, \omega) \equiv \frac{\partial \psi}{\partial x}\frac{\partial \omega}{\partial y} - \frac{\partial \psi}{\partial y}\frac{\partial \omega}{\partial x}, \quad \mathcal{M} \equiv \frac{\partial^2}{\partial x^2} + \frac{\partial^2}{\partial y^2}.$$

Here, $\mathcal{M}$ is the two-dimensional Laplacian and $\mathcal{N}$ represents the nonlinear term.

The assumed infinitely extended flow field is approximated by the finite domain indicated by ABCD in figure 1. Uniform flow is assumed to come to the upstream boundary (AB), and the outlet condition at the downstream boundary (CD) is approximated by the Sommerfeld radiation condition, which is expressed as

$$\frac{\partial \psi}{\partial t} + c\frac{\partial \psi}{\partial x} = 0, \quad \frac{\partial \omega}{\partial t} + c\frac{\partial \omega}{\partial x} = 0, \tag{2.3}$$

where the value of the nominal phase velocity c is evaluated numerically. The condition on the side boundaries AD and BC is also uniform flow. The no-slip condition is applied on the surface of each circular cylinder, written as

$$\psi = \psi_s, \quad \omega = -\frac{\partial^2 \psi}{\partial n^2}, \tag{2.4}$$

where n is the coordinate taken normal to the surface of the cylinders. These conditions are not sufficient for the unique determination of the solution of equations (2.1) and (2.2), unless the value of ψ_s is specified. In order to evaluate the value of ψ_s, we impose the condition that the pressure should be single-valued throughout the whole flow field, which is written as

$$\oint_C \nabla p \cdot \boldsymbol{t}\, \mathrm{d}s = 0, \tag{2.5}$$

where s and $\boldsymbol{t}$ are the coordinate and the tangential unit vector, respectively, along a path C that may be taken arbitrarily to surround each cylinder. However, we take the path C along the surface of each cylinder because the pressure gradient ∇p on

the surface is simply expressed as

$$\nabla p = -\frac{1}{Re}\nabla \times \boldsymbol{\omega} \tag{2.6}$$

owing to the no-slip condition applied on it.

3. Steady-state solution

At small Reynolds numbers, the flow is steady and symmetric with respect to the x-axis, i.e. the streamwise centreline through the middle of the gap between the two cylinders. The solution corresponding to the steady symmetric flow satisfies basic equations (2.1) and (2.2) under the boundary conditions, irrespective of the value of the Reynolds number, although it becomes unstable above a critical value. This steady symmetric flow, say $(\bar{\psi}, \bar{\omega})$, is the main flow for the linear stability analysis. The main flow is obtained numerically by solving the steady–state vorticity transport equation:

$$\mathcal{N}(\bar{\psi}, \bar{\omega}) + \frac{1}{Re}\mathcal{M}\bar{\omega} = 0, \tag{3.1}$$

which is obtained by dropping the term including the time-derivative in equation (2.1), together with the Poisson equation:

$$\bar{\omega} = -\mathcal{M}\,\bar{\psi} \tag{3.2}$$

under the same boundary conditions for (ψ, ω) in equations (2.4)–(2.6), except for the Sommerfeld boundary conditions at the outlet, which are reduced to $\partial\psi/\partial x = 0$ and $\partial\omega/\partial x = 0$.

4. Linear stability analysis

In order to analyse the linear stability of the steady symmetric flow (main flow), we consider a disturbance (ψ', ω') added to the main flow $(\bar{\psi}, \bar{\omega})$ and express the vorticity and the stream function as

$$\psi = \bar{\psi} + \psi', \quad \omega = \bar{\omega} + \omega', \tag{4.1}$$

respectively. Substituting these expressions into equation (2.1) and subtracting equation (3.1), we obtain a nonlinear disturbance equation for the vorticity disturbance ω' as

$$\frac{\partial\omega'}{\partial t} = \frac{1}{Re}\mathcal{M}\omega' + \mathcal{N}(\psi', \bar{\omega}) + \mathcal{N}(\bar{\psi}, \omega') + \mathcal{N}(\psi', \omega'). \tag{4.2}$$

Neglecting the nonlinear term of the disturbance (ψ', ω') in equation (4.2) and assuming the time dependence of the disturbance as $\psi' = \hat{\psi}(x, y)\mathrm{e}^{\lambda t}$ and $\omega' = \hat{\omega}(x, y)\mathrm{e}^{\lambda t}$, we arrive at a linearlized disturbance equation:

$$\lambda\hat{\omega} = \frac{1}{Re}\mathcal{M}\hat{\omega} + \mathcal{N}(\hat{\psi}, \bar{\omega}) + \mathcal{N}(\bar{\psi}, \hat{\omega}), \tag{4.3}$$

which is solved together with the Poisson equation for the disturbance:

$$\hat{\omega} = -\mathcal{M}\hat{\psi}. \tag{4.4}$$

Here, the coefficient λ is a complex linear growth rate of the disturbance, whose real and imaginary parts, λ_r and λ_i, are the growth rate and the frequency (angular velocity) of the disturbance, respectively. The steady symmetric flow is unstable if λ_r

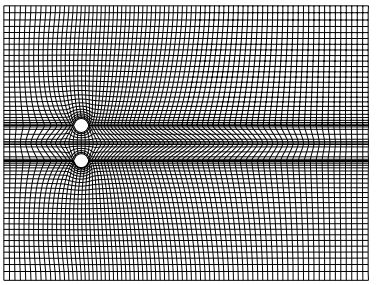

FIGURE 2. An example of the computational grid. $\Gamma = 1.5$.

is positive, or stable if λ_r is negative. Hence, the Reynolds number at which $\lambda_r = 0$ gives the critical value Re_c.

The boundary condition for $(\hat{\psi}, \hat{\omega})$ on the upstream and side boundaries is $(\hat{\psi}, \hat{\omega}) = (0, 0)$. The outlet condition on the downstream boundary is the Sommerfeld radiation condition. The no-slip boundary condition is applied on the surface of each circular cylinder, written as

$$\hat{\psi} = 0, \quad \hat{\omega} = -\frac{\partial^2 \hat{\psi}}{\partial n^2}. \tag{4.5}$$

Equations (4.3) and (4.4) constitute an eigenvalue problem under the boundary condition, for which infinite number of eigenvalues exist. We call each eigenvalue and/or eigenfunction a mode of instability.

5. Numerical method

We use two different numerical methods, one of which is numerical simulation of the basic equations (2.1) and (2.2) under the boundary conditions and an appropriate initial condition, and the other the linear stability analysis of the steady symmetric flow. In both methods, the spatial derivatives are approximated by finite differences in a curvilinear numerical grid generated to fit the circular cylinders. In order to generate the numerical grid, solutions of the following Poisson equations are adopted:

$$\frac{\partial^2 \xi}{\partial x^2} + \frac{\partial^2 \xi}{\partial y^2} = P(\xi, \eta), \quad \frac{\partial^2 \eta}{\partial x^2} + \frac{\partial^2 \eta}{\partial y^2} = Q(\xi, \eta). \tag{5.1}$$

Here, (ξ, η) are coordinates in the calculation space, and the source terms $P(\xi, \eta)$ and $Q(\xi, \eta)$ are utilized to cluster grid points near the surface of the cylinders. We determine the forms of $P(\xi, \eta)$ and $Q(\xi, \eta)$ with the technique proposed by Steger & Sorenson (1979). One of coordinates, η, is taken to be normal to the surface of the cylinders on which $\eta = 0$, while the other ξ is along the surfaces. The numerical domain is defined as $L_1 = 5d$, $L_2 = 40d$ and $L_3 = \ell/2 + 9d$, which must be large enough not to affect the numerical results (see figure 1). An example of the grid thus generated is shown in figure 2 for $\Gamma = 1.5$, with total number of mesh points 199×410; the minimum mesh size is $0.01d$ near the surfaces of the cylinders and the maximum size is $0.1d$ near the outlet and side boundaries, as shown in figure 2. The purpose of this is to take the fact that velocity field must change rapidly near the cylinder into consideration.

In numerical simulations of equations (2.1) and (2.2), we use the fourth-order Runge–Kutta method to approximate the time derivative, together with the second-order accuracy of central finite difference in space. Poisson equation (2.2) is solved by

the successive over-relaxation (SOR) method, in which the relaxation factor is usually taken as $\epsilon = 1.5$, although other values are also taken depending on the values of the Reynolds number and the gap ratio. The convergence of the solution for the Poisson equation is determined when the total relative difference in (ψ, ω) between two subsequent iterations at all the mesh points in the whole numerical domain is less than 10^{-7}. The flow is judged to have attained its steady state when the summations of the relative differences of ψ and ω between two subsequent time steps become smaller than 10^{-10}.

The SOR iterative method is also utilized in order to obtain the steady-state solution (the main flow) and also to solve the eigenvalue problem in the linear stability analysis. The steady-state solution is obtained numerically by solving equations (3.1) and (3.2) under the boundary conditions, where the spatial derivatives are approximated by the second-order finite differences. The antisymmetry of $(\bar{\psi}, \bar{\omega})$ with respect to the x-axis, i.e. $\bar{\psi}(x, -y) = -\bar{\psi}(x, y)$ and $\bar{\omega}(x, -y) = -\bar{\omega}(x, y)$, is taken into consideration in calculating the steady-state solution in order to save computation time. In the SOR iterative method to solve the eigenvalue problem in the linear stability analysis, the spatial derivatives are approximated by second-order finite differences. Here, the eigenfunctions $(\hat{\psi}, \hat{\omega})$ of the most growing mode have the symmetry $\hat{\psi}(x, -y) = \hat{\psi}(x, y)$ and $\hat{\omega}(x, -y) = \hat{\omega}(x, y)$, which can be utilized in numerical calculation.

6. Numerical results

We performed numerical simulations of the flow as well as linear stability analyses of the main flow mainly in the range of $Re \leqslant 80$ and $0.3 \leqslant \Gamma \leqslant 1.0$, and found that the flow characteristics drastically change around $\Gamma \sim 0.5 - 0.62$. Hence, we show the flow patterns and its transitions for $\Gamma = 0.5$, 0.6 and 0.62 as typical cases.

Steady symmetric flow is realized irrespective of its initial condition at small Reynolds numbers for any value of the gap ratio Γ, which is a unique steady-state solution of the governing equations. An example of steady symmetric flow is shown for $Re = 20$ and the gap ratio $\Gamma = 0.5$ in figure 3(*a*), in which the flow field is depicted only in the range of $x = [-5, 20]$ and $y = [-9.5, 9.5]$ although the numerical domain is larger in the downstream direction. In this figure, we observe a recirculation region at a small distance from the pair of cylinders. The recirculation region resembles the vortex pair behind a circular cylinder in a uniform flow though the vortex pair is attached to the cylinder whereas it is not attached here. However, if we regard the pair of cylinders as a single object having the same extent, we may consider the recirculation region to be similar to the twin-vortex though it is not attached.

In the case of $\Gamma = 0.5$, the first instability of the steady symmetric flow is caused by an oscillatory mode as seen in figure 3(*b*) for $Re = 50$, whose frequency f, i.e. the Strouhal number St in the present normalization, is about 0.069. The oscillation is observed beyond the downstream end of the recirculation region, whereas oscillation appears just behind the vortex pair in the flow past a single cylinder. However, we can find similarity between the two flows if we recall that the recirculation region behaves as a vortex pair. Thus we confirm that the oscillatory flow behind the pair of cylinders resembles the flow past a single virtual large object, so that we can call the flow a single bluff-body flow and the instability mode a far-downstream mode, respectively. Note that the oscillatory region for the far-downstream mode may extend upstream to just behind the two cylinders for larger Reynolds numbers than $Re = 50$.

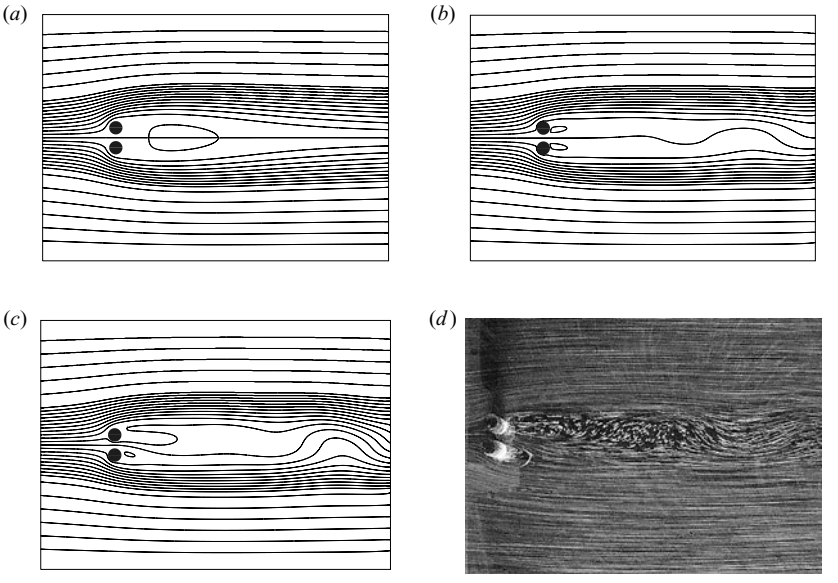

FIGURE 3. Flow pattern (streamlines) and experimental visualization of the flow. $\Gamma = 0.5$. (*a*) Steady symmetric flow. $Re = 20$. (*b*) Oscillatory flow. $Re = 50$. (*c*) Deflected oscillatory flow. $Re = 60$. (*d*) Deflected oscillatory flow (visualization from an experiment). $Re = 60$.

The second instability appears as a deflection of the stream through the gap between the cylinders. Figure 3(*c*) shows a flow pattern at $Re = 60$, in which we observe a deflection in the near wake of the cylinders together with oscillation far downstream. The mean flow over an oscillation period is asymmetric with respect to the streamwise centreline through the gap. A similar deflected flow pattern was reported for $Re = 70$ and $\Gamma = 0.5$ by Kang (2003). However, such a deflected flow was not expected to appear because it was believed that flow past symmetrically arranged obstacles would have the same symmetry in the mean even if it becomes oscillatory. Hence, we confirmed the deflected flow pattern in an experiment (figure 3*d*). The flow pattern was visualized by adding orgasol powder with density of $1.03\,\mathrm{g\,cm^{-3}}$ and $48 - 52\,\mu\mathrm{m}$ in diameter in water. The picture was taken at $Re \sim 60$ by a digital camera (Nikon D100), in which bright dots and lines are reflections of slit light from the orgasol powder.

We obtained a deflected oscillatory flow with $St \sim 0.074$ at $Re = 60$. The oscillation in the flow was observed significantly far from the two cylinders. In order to explore the origin of the deflection and oscillation in the flow, we take the velocities v_1 and v_2, the component in the y-direction at two points labelled by P_1 and P_2 in figure 1 which are located $2d$ and $14d$ from the pair of cylinders, as the representative physical quantities to demonstrate the change in the flow field. The histories of v_1 and v_2 are depicted in figure 4(*a*) for $Re = 50$. In figure 4(*a*), the oscillation amplitude of v_2 (broken line) is large, whereas v_1 is almost constant, which indicates that the oscillation is confined in a limited region from the cylinders. Although the oscillation amplitude of v_1 is small even at $Re = 60$, the mean value of v_1 is negative definite, which shows that the flow is deflected behind the cylinders. Thus it was found that the flow displays different characteristics at the two points.

The different behaviour of flow in the two regions may be confirmed by depicting the flow field of the disturbance, which is obtained by subtracting the steady symmetric

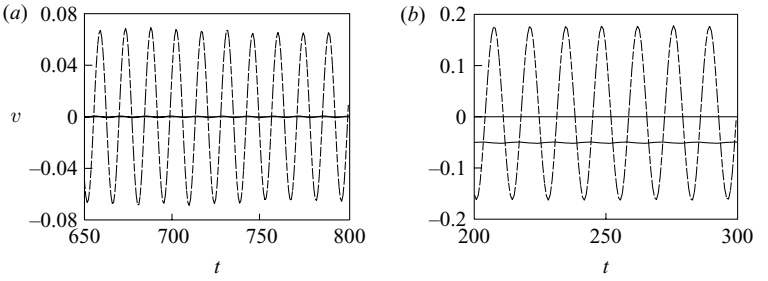

FIGURE 4. History of the velocities v_1 (P_1) and v_2 (P_2). Solid line: v_1, broken line: v_2. $\Gamma = 0.5$. (*a*) $Re = 50$, (*b*) $Re = 60$.

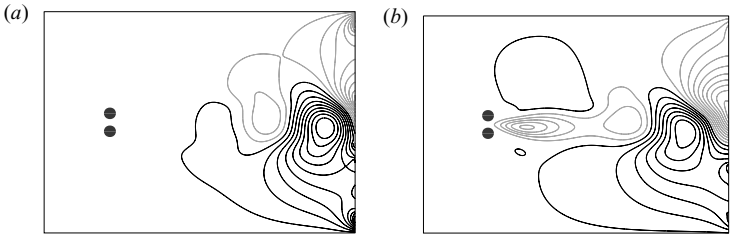

FIGURE 5. Flow pattern of disturbance (streamlines). Solid lines: positive values of $\psi - \bar{\psi}$, dashed lines: negative values of $\psi - \bar{\psi}$. $\Gamma = 0.5$. (*a*) $Re = 50$, (*b*) $Re = 60$.

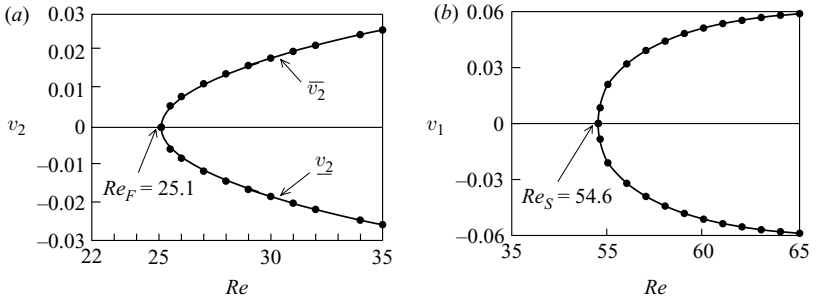

FIGURE 6. Bifurcation diagram. $\Gamma = 0.5$. (*a*) Hopf bifurcation, (*b*) pitchfork bifurcation.

flow (the main flow) from the instantaneous flow field of the oscillatory or oscillatory deflected flows. The flow patterns of the disturbance thus obtained are shown in figures 5(*a*) and 5(*b*) for $Re = 50$ and 60, in which solid and dashed lines show streamlines with positive and negative values of ψ, respectively. It is seen that the oscillatory disturbance has significant magnitude only in a confined region which is located about $13d \sim 19d$ downstream from the cylinders at $Re = 50$ (figure 5*a*). A stationary disturbance appears just behind the cylinders extending from the gap between the cylinders to the head of the oscillatory disturbance (about $12d$ behind the cylinders) at $Re = 60$ (figure 5*b*), which has elliptical contours elongated in the streamwise direction. Comparing these two figures, the distinction between the two regions in which the two disturbances have significant magnitude is apparent.

We also use the velocities v_1 and v_2 to analyse the bifurcation structure of the flow. Figure 6(*a*) shows the amplitude (maximum and minimum values, $\overline{v_2}$ and $\underline{v_2}$, in one period) of v_2 in periodic oscillation. From the relation of $|\overline{v_2} - \underline{v_2}| \propto (Re - Re_F)^{1/2}$,

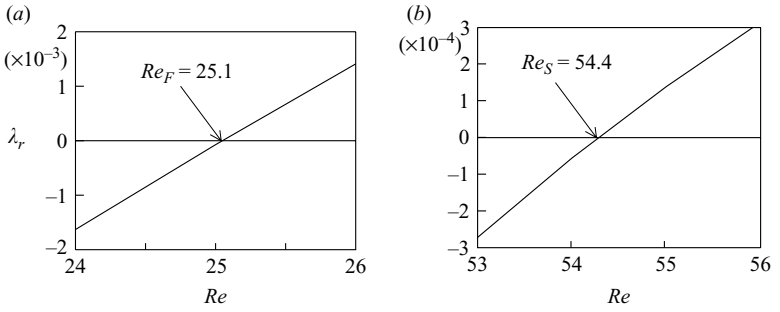

FIGURE 7. Linear growth rate λ_r. $\Gamma = 0.5$. (*a*) Far-downstream mode (Hopf bifurcation), (*b*) stationary mode (pitchfork bifurcation).

the bifurcation is judged to be a Hopf bifurcation with the critical Reynolds number $Re_F = 25.1$. The magnitude of v_1 is depicted in figure 6(*b*), because the flow is almost steady and deflected near the cylinders. It is seen in this figure that two solution branches bifurcate from the steady symmetric state, one of which has a positive value of v_1 and the other a negative value. It is the deflected flow with the negative value of v_1 that was depicted in figure 3(*c*), which is apparent also in figure 4(*b*). The other deflected flow with a positive value of v_1 may be obtained if another appropriate initial condition is adopted in numerical simulation. We confirmed from this figure that the bifurcation is a pitchfork bifurcation stemming from the steady symmetric state and evaluated the critical Reynolds number as $Re_S = 54.6$ by extrapolation using the relation $|v_1| \propto (Re - Re_S)^{1/2}$.

It may seem strange that the pitchfork bifurcation occurs at a larger Reynolds number than the critical value for the Hopf bifurcation although we concluded that the two different bifurcations occur in separate regions. To justify our conclusion, we analysed the linear stability of the main flow (steady symmetric flow). We obtained the main flow $(\bar{\psi}, \bar{\omega})$ numerically by solving equations (3.1) and (3.2) for each value of Re under the appropriate boundary condition, and solved the eigenvalue problem which consists of equations (4.4) and (4.5) together with the boundary conditions.

The eigenvalue λ for the most unstable mode of instability is found by the linear stability analysis to be complex. This mode, the far-downstream mode, is an oscillatory mode leading to the Hopf bifurcation, and it is easily proved that the complex conjugate λ^* is also an eigenvalue (the second mode) of the eigenvalue problem. The real part λ_r of the eigenvalue is depicted in figure 7(*a*). From this figure, the critical Reynolds number Re_F at which $\lambda_r = 0$ was determined as $Re_F = 25.1$. The critical value agrees with that evaluated by the bifurcation analysis within the accuracy of three digits. The imaginary part λ_i shows the angular velocity of the disturbance, from which the Strouhal number St, or the frequency of oscillation in the flow, is calculated from $St = \lambda_i/(2\pi)$. The value was evaluated as $St \sim 0.058$ for $\Gamma = 0.5$ in the range of Reynolds number ($\sim Re_F$) depicted in figure 7(*a*). The third mode is a stationary mode to induce the pitchfork bifurcation, having a real eigenvalue ($\lambda_i = 0$). The eigenvalue for the stationary mode of instability is depicted in figure 7(*b*), from which the critical Reynolds number is determined as $Re_S = 54.4$. This value also agrees well with $Re_S = 54.6$ evaluated from the bifurcation analysis. Thus it was confirmed that the two different bifurcations occur in separate regions in the whole flow field, which are represented by the points P_1 and P_2. We conclude that the

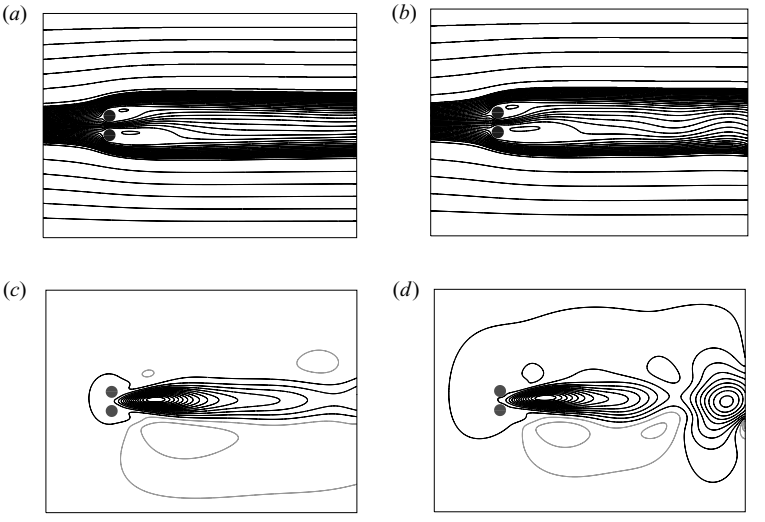

FIGURE 8. Flow pattern (streamlines). $\Gamma = 0.6$. (*a*) Steady asymmetric flow. $Re = 57$. (*b*) Deflected oscillatory flow. $Re = 60$. (*c*) Disturbance induced by instability due to stationary mode. $Re = 57$. (*d*) Disturbance induced by sequential instabilities due to stationary and oscillatory modes. $Re = 60$.

deflected flow reported by Kang (2003) is caused by the stationary mode of instability leading to a pitchfork bifurcation.

For a larger gap ratio, $\Gamma = 0.6$, an asymmetric steady flow is attained in the numerical simulation irrespective of the initial condition at $Re = 57$, as shown in figure 8(*a*), in which the stream through the gap between the two cylinders is observed to deflect toward one of the cylinders. The flow becomes oscillatory at $Re = 60$, yielding a deflected oscillatory flow with $St \sim 0.113$ (figure 8*b*). The critical Reynolds numbers for the pitchfork and Hopf bifurcations were determined as $Re_S = 55.2$ and $Re_F = 57.5$ from the bifurcation analyses of the numerical data. The critical values for the two bifurcations should be compared with $Re_S = 54.8$ and $Re_F = 57.3$ obtained by the linear stability analysis. Thus the two instabilities due to the stationary and oscillatory modes have swapped places between $\Gamma = 0.5$ and 0.6. The linear stability analysis shows that the flow also becomes unstable to another oscillatory mode which induces an in-phase oscillation behind the two cylinders. We call the instability mode an in-phase oscillation mode. Though the critical Reynolds number $Re_I = 55.8$ for the in-phase oscillation mode of instability evaluated by the linear stability analysis is smaller than Re_F, the amplitude of the in-phase mode is much smaller than that of far-downstream mode in the simulation results at $Re = 60$, which we confirmed by depicting the flow field of the disturbance. We show the flow patterns of the disturbance in figures 8(*c*) and 8(*d*) for $Re = 57$ and 60, respectively. The disturbance depicted in figure 8(*c*) is stationary, and extends from the gap between the cylinders to about $20d$ downstream, whereas the disturbance in figure 8(*d*) has an oscillatory part far downstream as well as the stationary part. The separation between the two regions in which the stationary and oscillatory disturbances have significant magnitude is clear in these figures.

The steady asymmetric flow is not attained at any value of Re for $\Gamma = 0.62$ in numerical simulation. The flow becomes oscillatory first with a gradual increase of the Reynolds number. We show a snapshot of the oscillatory flow pattern at $Re = 55$ in

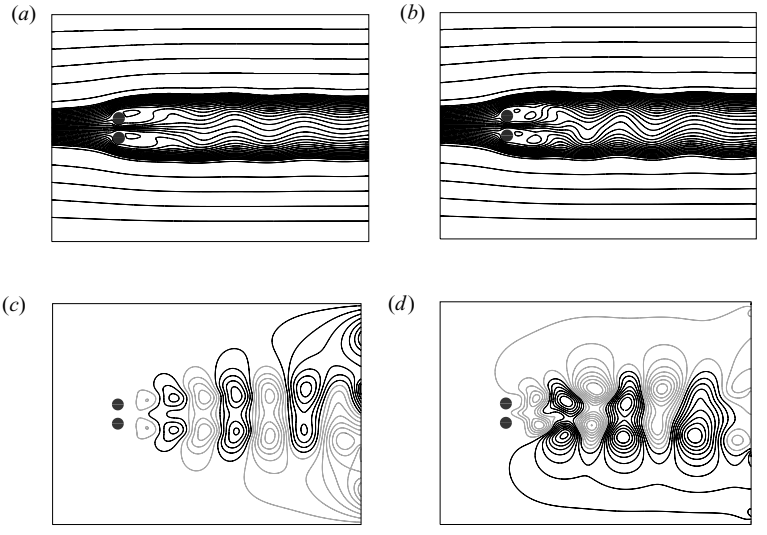

FIGURE 9. Flow pattern (streamlines). $\Gamma = 0.62$. (*a*) In-phase synchronously oscillating flow. $Re = 55$. (*b*) Deflected oscillatory flow. $Re = 60$. (*c*) Disturbance induced by instability due to the oscillatory in-phase mode. $Re = 55$. (*d*) Disturbance induced by sequential instabilities due to the oscillatory in-phase and stationary modes. $Re = 60$.

figure 9(*a*), in which the wakes behind the cylinders oscillate synchronously in the same phase and the oscillation is observed immediately behind the cylinders, in contrast to figure 3(*b*) where oscillation occurs far downstream from the cylinders. Taking the velocity v_2 as in figure 6(*a*), we depict a bifurcation diagram and identified a Hopf bifurcation with the critical Reynolds number $Re_I = 54.5$. The oscillatory disturbance yielding the Hopf bifurcation is the in-phase mode of instability. We carried out numerical calculations with the SOR method to trace the steady asymmetric flow found for $\Gamma = 0.6$, and confirmed the existence of pitchfork bifurcation with the critical Reynolds number $Re_S = 55.4$ also for $\Gamma = 0.62$. Note that such a steady asymmetric flow is not realized in experiment or numerical simulation. However, the influence of the pitchfork bifurcation appears in the flow pattern at $Re = 60$ (figure 9*b*), although the deflection is too small to clearly distinguish the asymmetry. In order to identify the instability mode and the asymmetry, we depict the flow fields of the disturbance $\hat{\psi}$ in figures 9(*c*) and 9(*d*) for $Re = 55$ and 60, respectively. It is seen in figure 9(*c*) that the flow field of the nonlinear disturbance at $Re = 55$ is almost symmetric with respect to the x-axis and that an array of paired vortices is aligned behind the two cylinders, whose sense of rotation is the same in each pair, but opposite in adjacent pairs in the array. This flow pattern of the disturbance shows that the mode is an in-phase oscillatory eigen mode. On the other hand, it is slightly asymmetric at $Re = 60$ due to the influence of the pitchfork bifurcation (figure 9*d*). The oscillation frequncy St is about 0.124 at $Re = 60$, which agrees well with the frequency $St \sim 0.124$ evaluated by the linear stability analysis at the critical Reynolds number ($Re_I = 54.7$, linear stability analysis).

Comparing the flow fields of the disturbance for $\Gamma = 0.6$ (figure 8*d*) and $\Gamma = 0.62$ (figure 9*d*) at the same Reynolds number $Re = 60$, we can easily see the difference between them. The disturbance field for $\Gamma = 0.6$ constitutes the stationary near-wake disturbance and an oscillatory far-downstream disturbance, whereas the oscillatory disturbance extends from the near-wake region into the entire downstream flow field

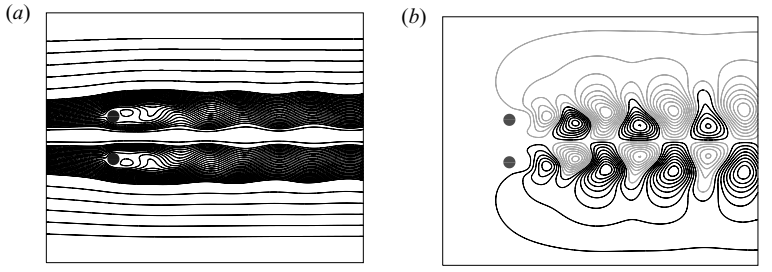

FIGURE 10. Antiphase synchronized oscillating flow (streamlines). $\Gamma = 2.5$, $Re = 50$. (a) Flow pattern, (b) disturbance.

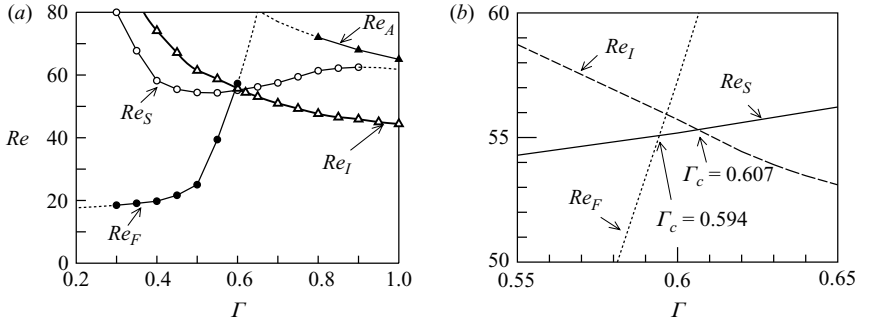

FIGURE 11. Transition diagram: ○, stationary mode; ●, far-downstream mode; △, in-phase mode; ▲, antiphase mode. (a) Whole diagram, (b) Enlargement of a part near $(\Gamma, Re) = (0.6, 55)$.

for $\Gamma = 0.62$. Hence, we conclude that the origins of the two disturbance fields are different and that the most unstable modes exchange in the very narrow range of $0.606 < \Gamma < 0.62$. The instability mode found for $\Gamma = 0.62$ was identified with one of the two kinds of synchronous oscillation mode, which was called an in-phase oscillation mode by Williamson (1985) and others. The other synchronous oscillation mode, i.e. an antiphase oscillation mode (antiphase mode) was also confirmed for larger gap ratios than $\Gamma \sim 0.8$ in our numerical simulation. One typical flow pattern of such oscillatory flows is shown in figure 10(a) for $\Gamma = 2.5$ and $Re = 50$. The disturbance field of the flow is depicted in figure 10(b), in which an array of paired vortices is observed behind the two cylinders similarly to figure 9(c), but the flow field significantly differs from 9(c) in that the sense of rotation in each pair is opposite. Thus the flow field of the disturbance is also symmetric with respect to the gap centreline, which is characteristic of the antiphase oscillatory mode. Note that the critical gap ratio for the exchange of in-phase and antiphase modes was evaluated as $\Gamma_c = 2.34$ by Akinaga & Mizushima (2005).

We made bifurcation analyses of the flow in the range of $0.3 \leqslant \Gamma \leqslant 1.0$ and evaluated the critical Reynolds numbers for the three oscillatory modes and the stationary mode of instability. The transition diagram thus obtained is shown in figure 11(a), where the critical Reynolds number for the far-downstream mode is indicated by the line with filled circles (Re_F) and the stationary mode by the line with open circles (Re_S). The lines with open triangles (Re_I) and with filled triangles (Re_A) indicate the criticality for the in-phase and antiphase oscillation modes, respectively. Figure 11(b) is an enlargement of the part of figure 11(a) where the three lines become

close together. Summarizing the first instability, for $\Gamma < 0.594$ the flow is unstable to the far-downstream mode. In the very narrow region of $0.594 < \Gamma < 0.607$, the stationary mode is the most unstable and for $0.607 < \Gamma < 2.34$ the in-phase oscillation mode becomes predominant over the other modes of instability. And the antiphase oscillation mode is the most unstable for $\Gamma > 2.34$, which leads to the symmetrically arranged vortex streets, as seen in figure 10(*b*).

Here, we should discuss on the possibility of observing two predominant oscillation frequencies in the flow. The oscillation we observed was always almost monotonic, having a single frequency. That is because we investigated the occurrence of the oscillation due to instability of the steady symmetric flow and the oscillation is monotonic just above the critical Reynolds number. We could identify the origin of the two distinct frequencies if two of the three oscillatory instability modes had oscillation frequencies that were multiples of the other. The oscillation in the flow at $Re = 60$ for $\Gamma = 0.6$ was induced solely by the far-downstream mode of instability, where the in-phase oscillation mode did not grow. The oscillation frequency for the far-downstream mode was obtained as $St \sim 0.113$ at $Re = 60$ for $\Gamma = 0.6$, and those for the in-phase and antiphase modes as $St \sim 0.125$ ($Re = 50$) and $St \sim 0.167$ ($Re = 76$), respectively, by numerical simulations. Thus, no pairs from the three have a simple integral ratio. Roughly estimating, the in-phase mode has a frequency $St \sim 0.12$ and the far-downstream mode $St \sim 0.07 - 0.08$. The far-downstream mode is thought to grow behind a unified bluff obstacle that is twice the cylinder diameter in size so that if we normalize the Strouhal number by $2d$, it becomes about $0.14 - 0.16$, which is a similar value to that of the in-phase mode. Hence, all three oscillation modes have a frequency of about $0.11 \sim 0.16$. We conjecture that the two predominant frequencies may occur at large Reynolds numbers, at least of several hundreds. In the paper by Akinaga & Mizushima (2005) in which cases of intermediate and large gap width of $\Gamma > 1$ were treated, the model of coupled oscillators proposed by Peschard & Le Gal (1996) was found not to predict the oscillation frequency in the antiphase and in-phase oscillatory flow. However, the model may have the potential to explain the appearance of simple integral ratios of frequencies for small gap width of $\Gamma < 1$.

For the case of a side-by-side arrangement of two cylinders, the lift and drag forces exerted on each cylinder are not significantly affected by the presence of the other cylinder in comparison with the case of a tandem arrangement. As the drag and lift forces were evaluated and fully discussed in terms of drag and lift coefficients C_D and C_L in the paper by Kang (2003) for small Reynolds numbers in the range of $40 \leqslant Re \leqslant 160$, we will not show our numerical results for C_D and C_L, which have a similar tendency. The flux through the gap between the two cylinders may be a more interesting physical quantity than the drag and lift forces. Hence, we evaluated the flux Q for each value of Γ at a constant Reynolds number, $Re = 60$. Figure 12 shows that the flux Q becomes virtually zero below $\Gamma_c \sim 0.11$ though Q is a linear function of Γ above the critical value. This suggests that the two cylinders with a gap narrower than this critical value behave like a solid body with width about twice the cylinder diameter. It is noted that the line for Q has slight kinks at $\Gamma = 0.607$ and 0.62, which is a sign of the change of the flow pattern beyond these gap ratios.

7. Discussion

Various flow patterns have been reported to appear in the flow past a pair of circular cylinders arranged side by side. However, the mechanism that produces each flow pattern has not been clarified. Our stability and transition analyses of the flow

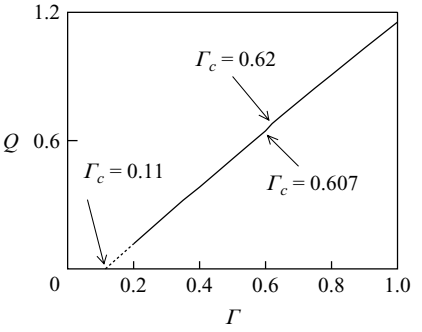

FIGURE 12. Flow rate through the gap between the cylinders.

revealed that the origins of these various flow patterns can be attributed to the linear instability of the steady symmetric flow, i.e. the basic flow, that is a unique solution at small Reynolds numbers. For instance, the deflected oscillatory flow was found to be a consequence of the sequential instabilities due to the far-downstream oscillation and the stationary modes. We have proved that the steady deflected flow originates from the instability of the basic flow due to the stationary mode, and found that it is realized in a very small parameter region of the gap ratio and the Reynolds number, though the effect of the pitchfork bifurcation is broad enough to deflect the flow even outside the patameter region. It is noted here again that the Coanda effect does not explain deflection of flow through a symmetrical path such as the gap between two circular cylinders symmetrically arranged.

We should explain how each mode of instability was distinguished in stability analysis, especially in the parameter region depiced in figure 11 in which several neutral curves intersect and the transition diagram is very complicated. We used a continuation method to trace each eigen mode, i.e. the set of eigenvalue and eigenfunction, by changing the values of the parameters in small increments. For example, the far-downstream mode is easily identified for $\Gamma = 0.3$. Hence we numerically calculated the eigen mode for a slightly larger value of Γ with the SOR iterative method in solving equations (4.3) and (4.4). Repetition of this numerical procedure gives the solution for each eigen mode successively. Needless to say, the in-phase oscillation mode must be calulated from a large value of Γ, i.e. $\Gamma = 1$.

We did not investigate nor confirm the flip-flopping flow because we conjecture that the origin of the flow will not be explained by the bifurcation analysis. Although the mechanism of occurrence of the flow has not been clarified in the present paper, it is thought to originate from a pair of asymmetric oscillatory flows. A steady asymmetric flow was observed at $Re = 57$ for $\Gamma = 0.6$ (figure 8*a*), which inevitably has a counterpart whose direction of deflection is opposite. Both of the flows are considered stable steady states as depicted schematically in figure 13, in which the states are indicated by x_1 and x_2. In numerical simulation, the flow will attain one of the two states depending upon its initial condition through a transient state. The steady flows become oscillatory due to the far-downstream oscillatory mode of instability as shown in figure 8(*b*) for $Re = 60$, which is the deflected oscillatory flow. The oscillatory states are depicted schematically in figure 13(*b*), where the oscillation of the flow is indicated by $x_1' - x_1''$ or $x_2' - x_2''$. Both the oscillatory states are also stable so that there exists a barrier between the two states. However, the barrier is easily overcome due to fluctuations which always exist in the flow field because

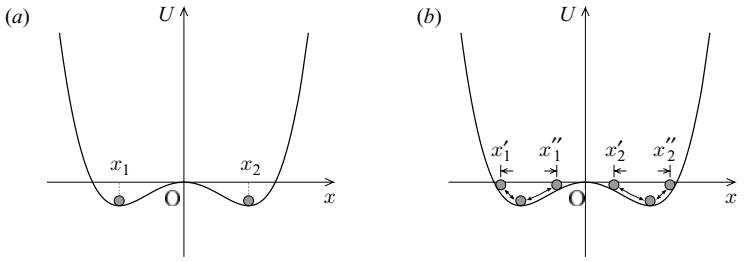

FIGURE 13. Schematic diagram explaining the mechanism of occurrence of the flip-flopping flow. (*a*) Asymmetric steady flow, (*b*) asymmetric oscillatory flow.

the oscillation amplitude becomes larger for larger Reynolds number. Then the flow oscillation overshoots to the other stable state, which results in the occurrence of the flip-flopping flow. The source of the fluctuations can be undulation of the oncoming flow in experiment or numerical errors in numerical simulation, which are thought to be random-like noise. Hence, the occurrence of the flip-flopping turns out to be a probabilistic Poisson process as described by Kim & Durbin (1988).

From our classification of instability modes, the six kinds of flow pattern found by Kang (2003) can be interpreted. The first two, i.e. the antiphase and in-phase oscillatory flows at $Re = 100$ for $\Gamma = 3.0$ and 1.5, come from the instability due to the corresponding near-wake oscillation modes, in-phase and antiphase oscillation modes, respectively. The flip-flopping pattern observed by Kang at $Re = 100$ for $\Gamma = 0.7$ is conjectured to originate from the deflected oscillatory flow as explained above. The single bluff-body pattern observed for $\Gamma = 0.2$ is induced due to the far-downstream mode of instability. The deflected steady flow appears after the instability due to the stationary disturbance. To be exact, the flow at $\Gamma = 0.5$ and $Re = 70$ depicted in figure 3(*e*) in Kang's paper is not a steady deflected, but a deflected oscillatory flow as clearly observed in the figure. The sixth pattern is the steady symmetric flow at low Reynolds numbers attained for any value of Γ.

We have assumed two-dimensional flow fields in the present paper. The critical Reynolds number for the two-dimensional flow to attain three-dimensional structure has not yet been obtained by experiments or numerical simulations for the side-by-side arrangement of cylinders, and may vary depending on the value of Γ. We speculate the critical value to be about $Re_c \sim 180$ for large gap width because the flow past a single cylinder is known to make a transition to three-dimensional flow at the value of $Re_c \sim 180$. Hence our numerical results, including the transition diagram depicted in the range of $Re \leqslant 80$, are valid without being affected by the appearance of three-dimensional flow structures.

We would like to thank Messrs Y. Yosuke, N. Suehiro, Y. Seki, K. Kawanishi, T. Moritani and Dr T. Akinaga for their help in numerical simulation and experiment.

REFERENCES

AGRAWAL, A., DJENIDI, L. & ANTONIA, R. A. 2005 Investigation of flow around a pair of side-by-side square cylinders using the lattice Boltzmann method. *Comput. Fluids* **35**, 1093–1107.

AKINAGA, T. & MIZUSHIMA, J. 2005 Linear stability of flow past two circular cylinders in a side-by-side arrangement. *J. Phys. Soc. Japan* **74**, 1366–1369.

BEARMAN, P. W. & WADCOCK, A. J. 1973 The interaction between a pair of circular cylinders normal to a stream. *J. Fluid Mech.* **61**, 499–511.

Ishigai, S., Nishikawa, E. & Cho, K. 1972 Experimental study on structure of gas flow in tube banks with tube axes normal to flow. *Bull. JSME* **15**, 949–956.

Kang, S. 2003 Characteristics of flow over two circular cylinders in a side-by-side arrangement at low Reynolds numbers. *Phys. Fluids* **15**, 2486–2498.

Kim, H. J. & Durbin, P. A. 1988 Investigation of the flow between a pair of circular cylinders in the flopping regime. *J. Fluid Mech.* **196**, 431–448.

Le Gal, P., Chauve, M. P., Lima, R. & Rezende, R. 1990 Coupled wakes behind two circular cylinders. *Phys. Rev.* A **41**, 4566–4569.

Le Gal, P., Peschard, I., Chauve, M. P. & Takeda, Y. 1996 Collective behavior of wakes downstream a row of cylinders. *Phys. Fluids* **8**, 2097–2106.

Mizushima, J. & Kawaguchi, Y. 2000 Transition of flow past a row of square bars. *J. Fluid Mech.* **405**, 305–323.

Mizushima, J. & Suehiro, N. 2005 Instability and transition of flow past two tandem circular cylinders. *Phys. Fluids.* **17** 104107-1–11.

Mizushima, J. & Takemoto, Y. 1996 Stability of the flow past a row of square bars. *J. Phys. Soc. Japan* **65**, 1673–1685.

Ohya, Y., Okajima, A. & Hayashi, M. 1988 Wake interference and vortex shedding. In *Encyclopedia of Fluid Mechanics* (ed. N. P. Cheremisinoff), vol. 8, pp. 323–389. Gulf.

Peschard, I. & Le Gal, P. 1996 Coupled wakes of cylinders. *Phys. Rev. Lett.* **77**, 3122–3125.

Ravoux, J. F., Nadim, A. & Haj-Hariri, H. 2003 An embedding method for bluff body flows: interactions of two side-by-side cylinder wakes. *Theor. Comput. Fluid Dyn.* **16**, 433–466.

Spivack, H. M. 1946 Vortex frequency and flow pattern in the wake of two parallel cylinders at varied spacings normal to the an air stream. *J. Aeronaut. Sci.* **13**, 289–297.

Steger, J. L. & Sorenson, R. L. 1979 Automatic mesh-point clustering near a boundary in grid generation with elliptic partial differential equation. *J. Comput. Phys.* **33**, 405–410.

Sumner, D., Wong, S. S. T., Price, S. J. & Païdoussis, M. P. 1999 Fluid behaviour of side-by-side circular cylinders in steady cross-flow. *J. Fluids Struct.* **13**, 309–338.

Williamson, C. H. K. 1985 Evolution of a single wake behind a pair of bluff bodies. *J. Fluid Mech.* **159**, 1–18.

Xu, S. J., Zhou, Y. & So, R. M. C. 2003 Reynolds number effects on the flow structure behind two side-by-side cylinders. *Phys. Fluids* **15**, 1214–1219.

Zdravkovich, M. M. 1977 Review of flow intererence between two circular cylinders in various arrangement. *Trans. ASMEI: J. Fluids Engng* **99**, 618–633.

Zdravkovich, M. M. & Pridded, D. L. 1977 Interference between two circular cylinders; series of unexpected discountinuities. *J. Ind. Aero.* **2**, 255–270.

Zhou, Y., Wang, Z. J., So, R. M. C., Xu, S. J. & Jin, W. 2001 Free vibrations of two side-by-side cylinders in a cross-flow. *J. Fluid Mech.* **443**, 197–229.

Zhou, Y., Zhang, H. J. & Yiu, M. W. 2002 The turublent wake of two side-by-side circular cylinders. *J. Fluid Mech.* **458**, 303–332.